



SOLAR PHYSICS

Picoflare jets power the solar wind emerging from a coronal hole on the Sun

L. P. Chitta^{1*}, A. N. Zhukov^{2,3}, D. Berghmans², H. Peter¹, S. Parenti⁴, S. Mandal¹, R. Aznar Cuadrado¹, U. Schühle¹, L. Teriaca¹, F. Auchère⁴, K. Barczynski^{5,6}, É. Buchlin⁴, L. Harra^{5,6}, E. Kraaikamp², D. M. Long^{7,8}, L. Rodriguez², C. Schwanitz^{5,6}, P. J. Smith⁷, C. Verbeek², D. B. Seaton⁹

Coronal holes are areas on the Sun with open magnetic field lines. They are a source region of the solar wind, but how the wind emerges from coronal holes is not known. We observed a coronal hole using the **Extreme Ultraviolet Imager on the Solar Orbiter spacecraft**. We **identified jets on scales of a few hundred kilometers, which last 20 to 100 seconds and reach speeds of ~100 kilometers per second**. The jets are powered by **magnetic reconnection and have kinetic energy in the picoflare range**. They are intermittent but widespread within the observed coronal hole. We suggest that **such picoflare jets could produce enough high-temperature plasma to sustain the solar wind and that the wind emerges from coronal holes as a highly intermittent outflow at small scales**.

Hot plasma continuously escapes the Sun into the heliosphere, forming the solar wind (1, 2). Fast solar wind streams (those with speeds $>500 \text{ km s}^{-1}$) have been traced to large (mostly polar) coronal holes—features formed by open magnetic fields on the Sun that appear dark in coronal images taken at extreme ultraviolet (EUV) or x-ray wavelengths (3–5). Small coronal holes that form adjacent to active regions (areas on the Sun with strong magnetic fields, including sunspots) could be the source regions of slower wind, with speeds $<500 \text{ km s}^{-1}$ (6, 7).

The physical origin and acceleration mechanism of solar wind from coronal holes are debated (5, 8, 9). Potential drivers include wave dissipation and turbulent cascades (10–12) or interchange reconnection between open and closed magnetic field lines at the coronal base (13–15). Jets with temperatures of $\sim 0.1 \text{ MK}$ emerge from the transition region network at the base of the corona (network jets), which are common in coronal hole regions, and could sustain the solar wind (16). Coronal counterparts to network jets are rare (17, 18), so it is unclear whether the cooler network jets can efficiently supply hot plasma to drive the solar wind.

Previous EUV imaging has shown signatures of jet outflows from plumes (bright raylike features embedded in coronal holes) and

the ambient, interplume coronal hole regions (19, 20). EUV images, with spatial resolution of $\sim 1000 \text{ km}$, have shown that plumes have substructures consisting of jets with widths as small as 1500 km (21–23). These jets appear to be universal in the corona: They emerge from coronal hole plumes, from quiet regions and from active regions of the Sun's atmosphere (24). Jets from plumes could sustain the solar wind mass flux during the minimum of the 11-year solar activity cycle and up to 60% of the mass flux during times of maximum activity (23). Because plumes fill only 10% of a coronal hole's volume (25), the bulk of the wind might originate in interplume regions (26–28). However, the spatial structure and timescales of interplume outflows are not known.

The solar wind emerging from coronal holes connects the Sun to the heliosphere. Spacecraft measurements in the inner heliosphere have been interpreted as showing that reversals of the radial magnetic field (known as switchbacks) in the solar wind are modulated on spatial scales as small as 1 Mm (the typical convective granular scale of the photosphere) at the base of the Sun's corona (29). However, EUV imaging has not been available with subgranular resolution ($<1 \text{ Mm}$), which is necessary to investigate this proposal.

EUV observations of a coronal hole

We observed a coronal hole using the EUV high-resolution imager (HRI_{EUV}), which is part of the Extreme Ultraviolet Imager (EUI) (30) instrument on the Solar Orbiter spacecraft (31). The passband of HRI_{EUV} is centered at 17.4 nm , with its thermal response function peaking at temperatures of $\sim 1 \text{ MK}$ because of emission lines of Fe IX (at 17.11 nm) and Fe X (at 17.45 and 17.72 nm).

The coronal hole was located close to the Sun's south pole. The data were obtained on 30 March 2022 between 04:30 and 05:00 universal time (UT) as part of an observing cam-

paign performed around perihelion (the close approach of the spacecraft to the Sun). The images have a spatial resolution of $\sim 237 \text{ km}$ on the Sun and a cadence of 3 s (32).

We split the coronal hole into three regions (labeled R1 to R3 in Fig. 1A) to investigate the small-scale coronal dynamics. Regions R1 and R3 are darker portions of the coronal hole with a few embedded brighter emission structures, known as coronal bright points, whereas R2 is an isolated plume within the coronal hole.

Y-shaped transient jets

We identify a Y-shaped jet with a base extent of $\sim 5 \text{ Mm}$ (between boxes R1-2 and R1-4 in Fig. 1B). Jets with such Y-shaped morphology are common in coronal holes (33). We focus on smaller jets, on spatial scales of $<1 \text{ Mm}$, emerging from the ambient coronal hole. We visually identified 10 such small-scale jets within R1 (Fig. 1, C to L). Some of these jets show a full or partial Y-shaped morphology (jets 1, 2, 3, 6, 7, 8, and 10), whereas others show a much simpler linear morphology (jets 4, 5, and 9). It is possible that all are intrinsically Y shaped, but the Y-shaped structure is not visible in some cases because of the viewing angle, which could lead to both legs of the jet being aligned with the line of sight. All of these jets have fine-scale structure down to the spatial resolution of our images.

These small jets exhibit intensity enhancements, over the background emission from the coronal hole. Figure 2 shows light curves of three example jets in region R1. For each of these, we selected two spatial points along the path of the jet to study the intensity variations (fig. S1). The intensity enhancements (defined as the amplitude of intensity fluctuations compared with the local background) are in the range of 100 to 300 digital numbers (DN) per pixel (equivalent to counts of ~ 15 to 44 photons per pixel; for comparison, coronal bright points in our observations are ~ 500 photons per pixel). Depending on the number of pixels used for spatial averaging of the signal, peak intensities of all these jets (above the background average intensity) are at least three times the local background photon noise (32).

The observed intensity fluctuations vary on timescales of 20 to 60 s (Fig. 2). Features associated with an intense jet base (Fig. 1, E to H) at least partially persist for longer timescales of 300 to 600 s but also exhibit intensity fluctuations on shorter timescales of 100 s. We estimate that the jet speeds are $\sim 100 \text{ km s}^{-1}$ with the speeds of different jets varying by a factor of 2 (Fig. 2, D to F) (32). These differences in measured jet speeds could be a result of projection effects. We observed repeated jet activity in these regions and visually counted a total of 38 small jets from the 10 locations

¹Max-Planck-Institut für Sonnensystemforschung, 37077 Göttingen, Germany. ²Solar-Terrestrial Centre of Excellence, Solar Influences Data Analysis Centre, Royal Observatory of Belgium, 1180 Brussels, Belgium. ³Skobel'syn Institute of Nuclear Physics, Moscow State University, Moscow 119991, Russia. ⁴Institut d'Astrophysique Spatiale, Centre National de la Recherche Scientifique, Université Paris-Saclay, 91405 Orsay, France. ⁵Physikalisch-Meteorologisches Observatorium Davos, World Radiation Center, 7260 Davos Dorf, Switzerland. ⁶Eidgenössische Technische Hochschule Zürich, 8093 Zürich, Switzerland. ⁷Mullard Space Science Laboratory, University College London, Dorking, Surrey RH5 6NT, UK. ⁸Astrophysics Research Centre, School of Mathematics and Physics, Queen's University Belfast, Belfast BT7 1NN, Northern Ireland, UK. ⁹Southwest Research Institute, Boulder, CO 80302, USA. *Corresponding author. Email: chitta@mps.mpg.de

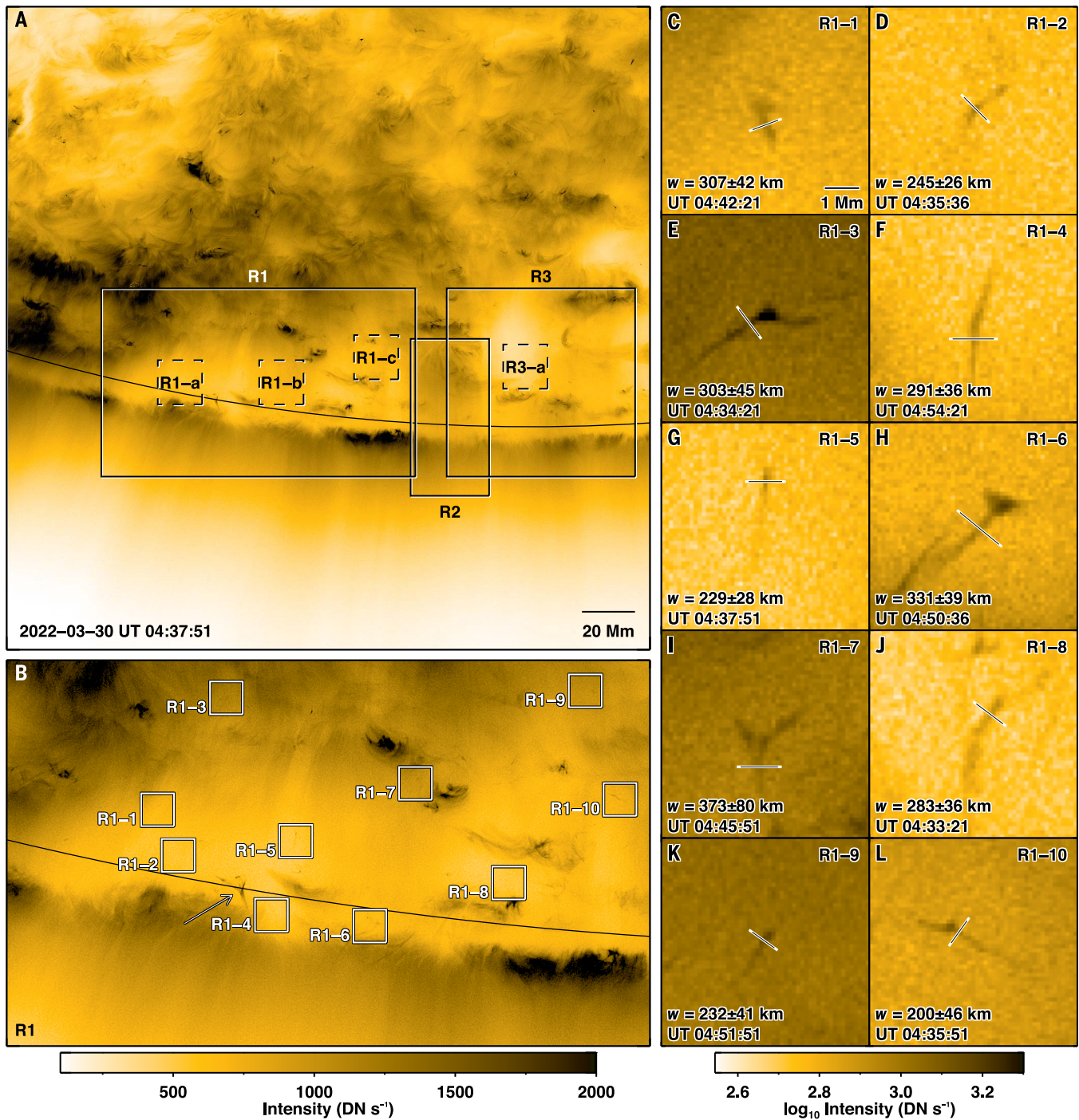


Fig. 1. EUV images of jets from a coronal hole. All images are displayed on a negative color scale (i.e., black is bright). Each panel shows data with a 15-s effective cadence (32), and south is roughly downward. **(A)** An overview HRLEUV image of a south polar coronal hole recorded on 30 March 2022 around 04:38 UT. The field of view is ~ 243 Mm \times 243 Mm. Solid boxes labeled R1 to R3 outline regions of the coronal hole discussed in the text. Dashed boxes labeled R1-a, R1-b, R1-c, and R3-a are interplume regions. The solid curve indicates the position of the Sun's limb.

(B) Zoomed-in view of R1 from **(A)** on the same brightness scale. Boxes labeled R1-1 to R1-10, each ~ 6 Mm \times 6 Mm, indicate locations within the coronal hole where we identified small-scale jet activity. The arrow points to an ~ 5 -Mm-scale-larger Y-shaped jet. An animated version of this panel is shown in movie S1. **(C to L)** Closer views of the boxes in **(B)** on a logarithmic brightness scale. White lines indicate locations where the width of each jet w was measured; its value is shown at the bottom of each panel (also listed in table S1).

labeled in Fig. 1 over the course of 30 min of observations. We also identified 29 additional small-scale jets in the wider coronal hole region (movie S1).

Plume-related jets

The emission from region R2 (Fig. 1A) is enhanced over the immediate surroundings, which suggests that it is a coronal hole plume.

We observed clusters of small jets emerging throughout the associated plume region (Fig. 3). These plume jets do not have the Y-shaped morphology of the jets discussed above.

Downloaded from https://www.science.org at National Astronomical Observatories, Cas on August 25, 2023

Previous lower-resolution EUV observations have shown that outflows from plumes are structured in the form of jets (21) and that the outflows are quasiperiodic in nature, with speeds of $\sim 100 \text{ km s}^{-1}$ (19, 23). Our higher-resolution HRI_{EUV} observations show even smaller jets, with cross-sectional widths close to the spatial resolution limit of $\sim 200 \text{ km}$ (a very thin jet is shown in Fig. 3H). We observe at least 30 such jets from the plume (movie S2).

Faint interplume emission and jets

Although both the interplume Y-shaped jets and the plume jets are spatially discrete, we found that there is a more widespread emission that is faint yet above the background level. This fainter emission, with veil-like morphology, exhibits apparent outward propagation throughout the coronal hole (fig. S3 and movies S3 and S4). The fainter emission also originates from the interplume regions; we designate four examples as R1-a, R1-b, R1-c, and R3-a (Fig. 1A). These regions of fainter emission are partially obscured by the foreground emission in R1, but the source region in R3 is unobscured.

This fainter, veil-like emission is also spatially structured. There are outflows apparently emerging from the identified source regions in the form of small-scale jets. Figure 4 shows three example jets from three of the identified interplume sources. Compared with the Y-shaped jets in Fig. 1, these interplume jets are even fainter; however, they are still at least three times the local background photon noise above the background mean intensities. These fainter jets exhibit intensity enhancements of $\sim 50 \text{ DN}$ per pixel over the local background (Fig. 4 and fig. S2). These interplume jets have similar morphology to that of the plume counterparts, and their cross-sectional widths are close to the resolution limit of the images. Interplume jets also appear in clusters on larger scales— $>10 \text{ Mm}$ —similar to plume jets. They are associated with intensity propagations; although we cannot determine these jet speeds because of noise, we constrain them to be supersonic outflows $>100 \text{ km s}^{-1}$ (32).

Magnetic origins of the jets

The high speeds, short timescales, and narrow widths of the observed jets indicate that they are driven by a variable energy source located at the coronal base, on spatial scales of $\lesssim 100 \text{ km}$. Y-shaped jets (Fig. 1) are already known to be driven by reconnection of open and closed magnetic field lines (34–36). The base width of $\lesssim 1 \text{ Mm}$ indicates that the observed small, Y-shaped jets are associated with the emergence or cancellation of granular-scale magnetic features (37). Although the plume and fainter interplume jets we observed on the solar disc do not have Y-shaped morphology, similar features ob-

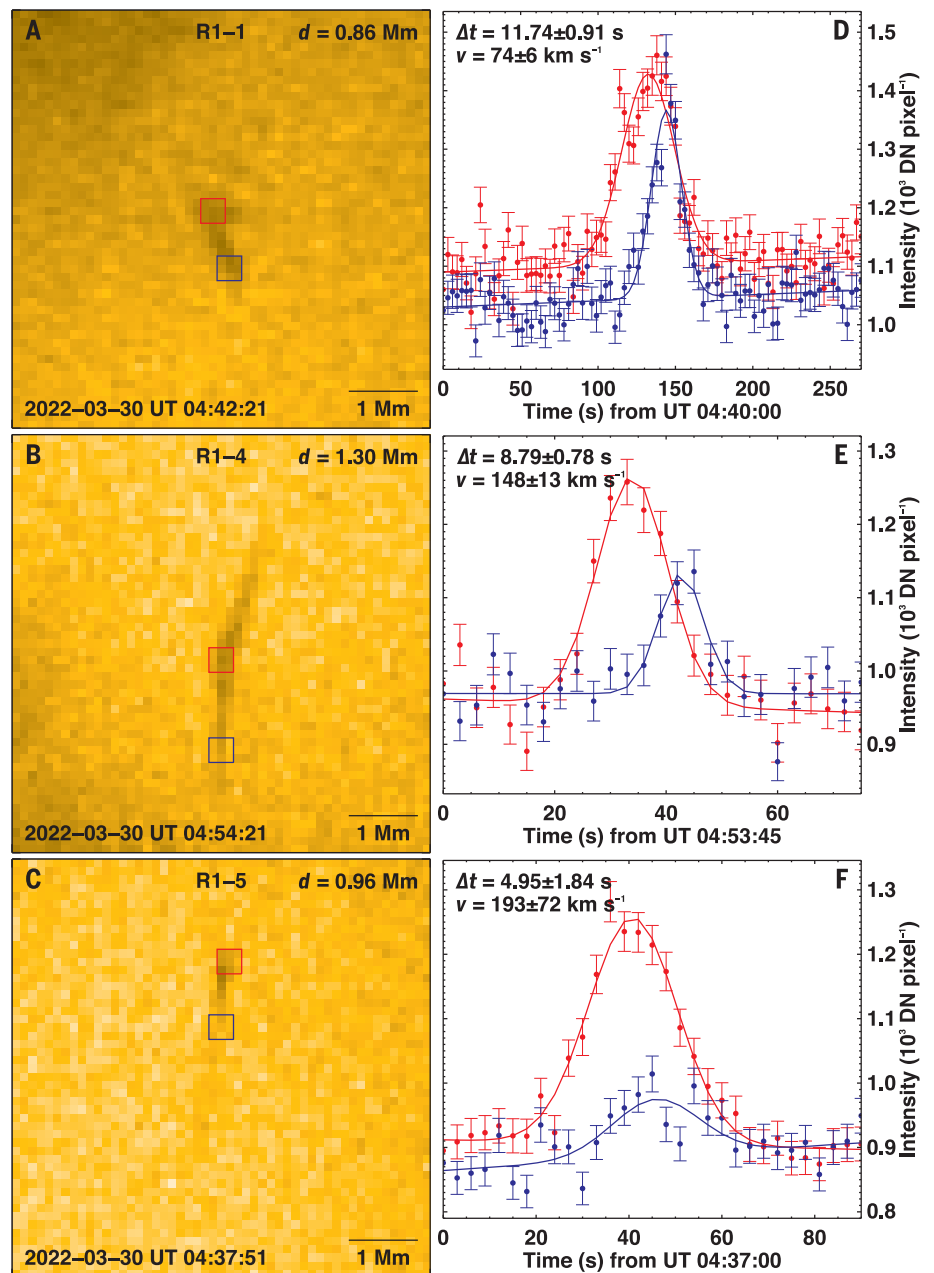


Fig. 2. Temporal variability in three example small-scale jets. (A to C) Same EUV images as Fig. 1, C, F, and G, respectively. The red and blue squares mark locations along each jet, separated by a plane-of-sky distance d listed in the top right of each panel. (D to F) Data points are average intensities within the corresponding red and blue boxes in (A) to (C) as a function of time, with a cadence of 3 s. Error bars indicate 1σ uncertainties because of photon Poisson (shot) noise (32). The red and blue solid curves are Gaussian models fitted to the observed intensities. The separation between the centroids of the two Gaussian peaks Δt and the speed $v = d/\Delta t$ (with their standard errors) are listed in each panel (also listed in table S2).

served on the Sun's limb do have morphologies consistent with the magnetic topology of interchange reconnection between open and closed magnetic domains (figs. S4 to S6 and movies S5 to S9). We therefore suggest that all the jets we observed are transiently driven by reconnection.

Previous observations have shown that the Ne VII emission line, which samples transition region and coronal plasma with temperatures

of $\sim 0.63 \text{ MK}$ and above, has systematic blueshifts indicating upward flows of $\sim 10 \text{ km s}^{-1}$ in coronal holes (13, 38). The outflow speeds in interplume regions can be up to 70 km s^{-1} (27, 28). The small-scale jets that we observed could be the $\sim 1\text{-MK}$ counterparts of the coronal hole outflows previously inferred through spectroscopy at lower spatial resolution. The high-speed jets driven by reconnection in our

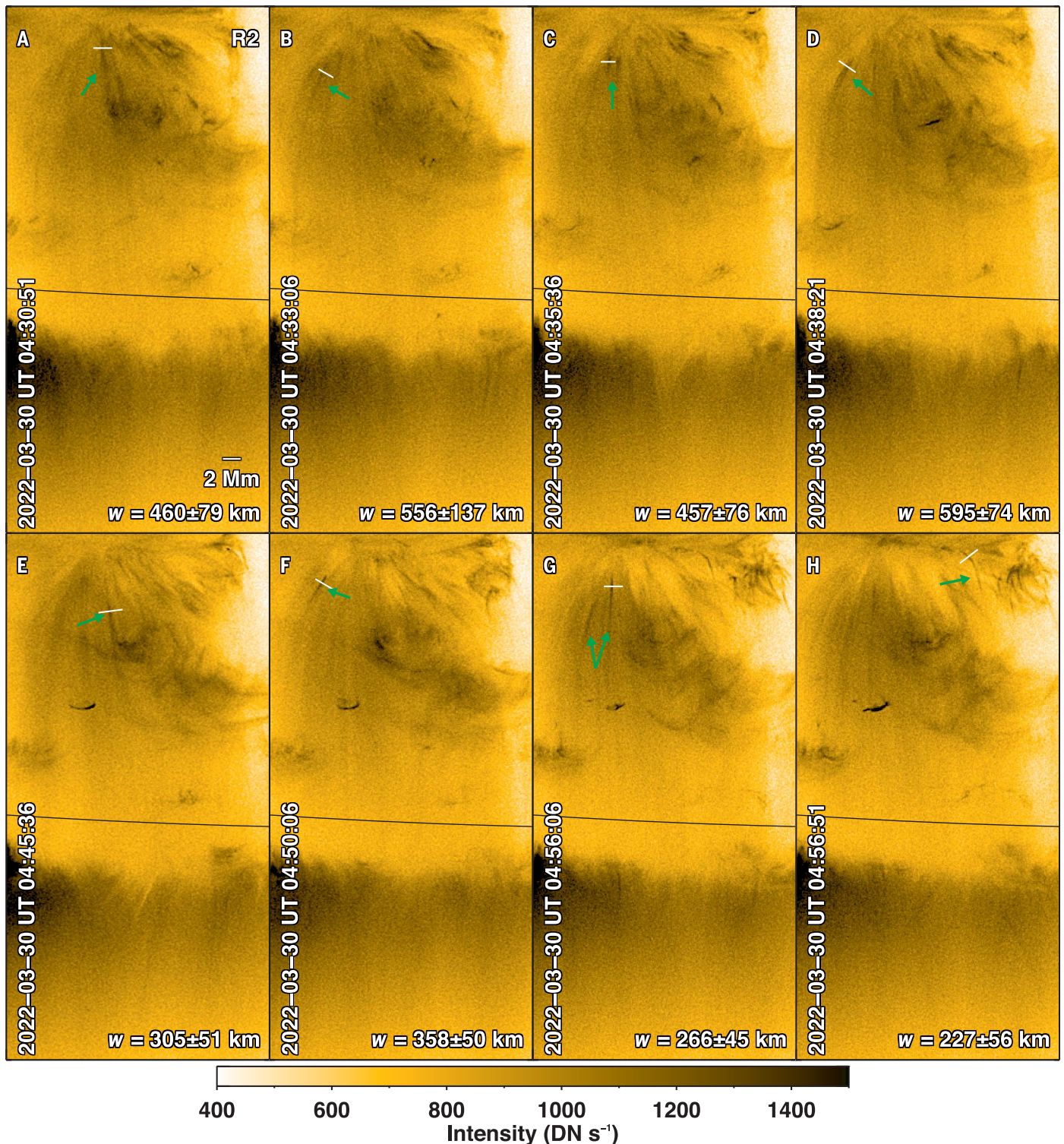


Fig. 3. Jets from plumes. (A to H) The panels all show region R2 from Fig. 1A but for different times (labeled on each image) with an effective cadence of 15 s (32). Small-scale jet activity is indicated by green arrows. White lines indicate locations where the cross-sectional width w of each jet was measured, with the results listed in each panel (also listed in table S3). The solid curve marks the solar limb. An animated version of this figure is shown in movie S2.

observations propagate outward and could channel some, if not all, of the material contained within the jets along the open magnetic field lines of the coronal hole, powering the solar wind.

We do not observe any signatures of downward flows in the jets. If they exist, they could be too weak to be detectable in our observations, or they might contain plasma at different temperatures to which the HRI_{EUV} instrument is not sensitive.

Jet energetics

Assuming that the apparent outflows we detected are mass motions, we estimate a lower limit on the kinetic energy flux of $\gtrsim 10^5$ erg cm⁻² s⁻¹ (32). This is probably an

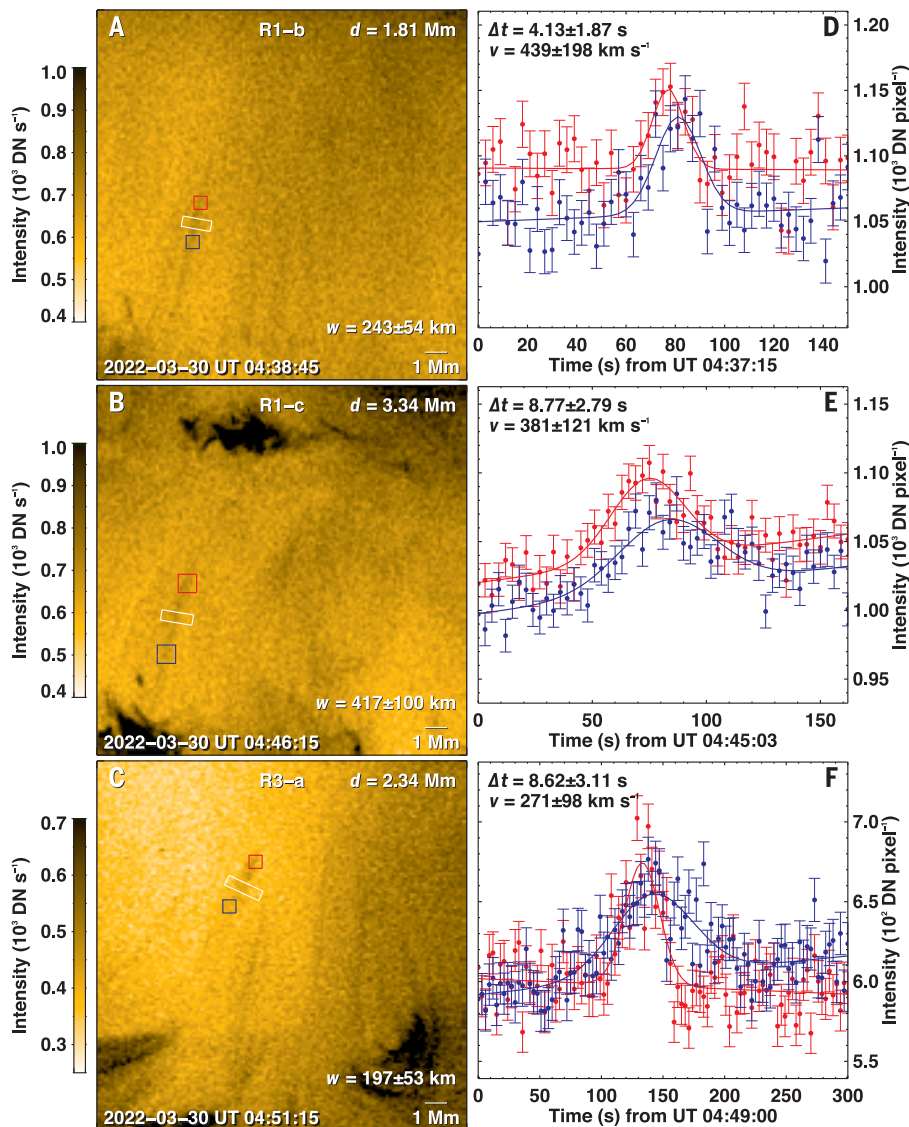


Fig. 4. High-speed faint jets from interplume regions. (A to F) Same as Fig. 2 but for the boxes labeled R1-b, R1-c, and R3-a in Fig. 1A. Cross-sectional width w of each jet was measured by averaging the intensity across the white strip, with the results listed in each panel. The images in (A) to (C) have an effective cadence of 30 s. The average intensities in (D) to (F) have a cadence of 3 s (32). Jet parameters are listed in table S4.

underestimate because of line-of-sight effects. Increasing the jet speed by a factor of 2 to 4 would increase the kinetic energy flux of a given jet by nearly one to two orders of magnitude.

Our estimate of the kinetic energy flux in these jets is similar to the minimum nonradiative energy input required to power magnetically open coronal regions (39). The narrowest jets we observed have cross-sectional widths of only a few pixels, corresponding to diameters of <237 km, assuming a cylindrical shape. The observed intensity fluctuations are on timescales of 20 to 100 s. If we take that to be the lifetime of the jet and combine it with the derived kinetic energy flux, we infer that the lower limit for the kinetic energy content of

a single narrow, faint jet is $\geq 10^{21}$ erg. The typical energy content of a nanoflare is 10^{24} erg (40), so the kinetic energy content of fainter interplume jets is in the picoflare range. We therefore refer to these features as picoflare jets. The Y-shaped jets (Fig. 1) and the plume jets (Fig. 3), which are somewhat brighter, presumably carry more kinetic energy.

Plasma outflows from picoflare jets, channeled along the open magnetic field lines of coronal holes, could contribute to the mass flux of the solar wind. We estimate the total mass-loss rate \dot{m} of the observed jets as $\dot{m} = 4\pi R_{\odot}^2 \rho v f_{\text{CH}} f_j$, where $R_{\odot} = 695$ Mm is the radius of the Sun, $\rho = 3.34 \times 10^{-16}$ g cm^{-3} is the jet mass density, $v = 100$ km s^{-1} is the jet speed (32), $f_{\text{CH}} \approx 0.1$ is the fractional area coverage of

coronal holes on the Sun (41), and f_j is the filling factor of picoflare jets. During periods of high solar activity, upward flows from the edges of active regions could also contribute to the solar wind mass flux (42–45). If picoflare jets account for the wind mass flux of $\sim 10^{12}$ g s^{-1} throughout the solar cycle (46), their filling factor f_j would need to be ~ 0.05 .

Our observations do not spatially resolve the smallest jets (32), especially those in the interplume regions that have weaker intensity enhancements and lower contrast with respect to the local background. Our results are consistent with previous EUV imaging at lower spatial resolution (24). The picoflare jets are common in our images (figs. S7 and S8), particularly in the interplume regions that cover a substantial portion of the coronal hole (movies S10 to S12). Above the limb, we observe persistent jet activity that fills the plane of sky (fig. S9). Any fainter jets would not be distinguishable from the background intensity fluctuations in our data.

Implications for the solar wind

Given their frequency in our observations, we suggest that these picoflare jets might be ubiquitous. If so, those emerging from the interplume regions, and to a lesser extent those from plume regions, could provide substantial plasma and energy flux to the solar wind throughout the solar cycle. This is consistent with previous suggestions that small jets make a substantial contribution to the solar wind (24).

The intermittent variability and short lifetimes (20 to 100 s) of the observed jets are consistent with the inherently ephemeral nature of magnetic reconnection. Our observations are not sensitive to any steady component of the solar wind. Nevertheless, we suggest that a dynamic component of the solar wind emerges from coronal holes as an intermittent outflow at the coronal base, which is observed as picoflare jets.

Neighboring small-scale, high-speed outflows with different speeds would produce a velocity shear, leading to instabilities (47, 48). We suggest that this could occur in both plume and interplume regions (32). If picoflare jets are ubiquitous, these instabilities could play a role in the formation of structures in the solar wind, such as magnetic switchbacks (7). In situ spacecraft measurements of the solar wind in the inner heliosphere have been interpreted as showing that the sources responsible for the large- and midscale modulation of switchbacks operate on spatial scales similar to the typical convective scales of granules and supergranules on the Sun (29). The narrow widths of the picoflare jets that we observed are compatible with them having underlying source regions of <1 Mm, which is smaller than the typical granule scale (49). The larger clusters of picoflare jets that we observed have structure

on scales >10 Mm, which is close to the super-granule scales of 10 to 60 Mm (50). Our interpretation that the picoflare jets are driven by granular-scale reconnection could therefore be related to the mid- to large-scale modulations of switchbacks in the solar wind.

The lifetimes and speeds of the **picoflare jets** are similar to those of network jets, which are common in the transition region (16), so the phenomena might be related. Our data cannot determine **whether a hot picoflare jet (~1 MK)** hosts plasma that has been heated from a cooler network jet phase or whether there are two populations of jets present simultaneously (colder network jets and hotter coronal picoflare jets). We suggest that picoflare jets could supply heated material to the solar wind as could the transition region jets if their energy is dissipated (16).

REFERENCES AND NOTES

1. E. N. Parker, *Astrophys. J.* **128**, 664 (1958).
2. M. Neugebauer, C. W. Snyder, *Science* **138**, 1095–1097 (1962).
3. J. Woch *et al.*, *Geophys. Res. Lett.* **24**, 2885–2888 (1997).
4. D. J. McComas *et al.*, *J. Geophys. Res.* **105**, 10419–10433 (2000).
5. S. R. Cranmer, *Living Rev. Sol. Phys.* **6**, 3 (2009).
6. Y.-M. Wang, Y.-K. Ko, *Astrophys. J.* **880**, 146 (2019).
7. S. D. Bale *et al.*, *Nature* **576**, 237–242 (2019).
8. G. Poletto, *Living Rev. Sol. Phys.* **12**, 7 (2015).
9. N. M. Viall, J. E. Borovsky, *J. Geophys. Res. Space Phys.* **125**, JA026005 (2020).
10. S. R. Cranmer, A. A. van Ballegoijen, R. J. Edgar, *Astrophys. J. Suppl. Ser.* **171**, 520–551 (2007).
11. T. Matsumoto, T. K. Suzuki, *Astrophys. J.* **749**, 8 (2012).
12. M. Shoda, B. D. G. Chandran, S. R. Cranmer, *Astrophys. J.* **915**, 52 (2021).
13. C.-Y. Tu *et al.*, *Science* **308**, 519–523 (2005).
14. L. Yang *et al.*, *Astrophys. J.* **770**, 6 (2013).
15. Y.-M. Wang, *Astrophys. J.* **904**, 199 (2020).
16. H. Tian *et al.*, *Science* **346**, 1255711 (2014).
17. P. Kayshap, K. Murawski, A. K. Srivastava, B. N. Dwivedi, *Astron. Astrophys.* **616**, A99 (2018).
18. J. Gorman, L. P. Chitta, H. Peter, *Astron. Astrophys.* **660**, A116 (2022).
19. H. Tian, S. W. McIntosh, S. R. Habbal, J. He, *Astrophys. J.* **736**, 130 (2011).
20. S. Pucci, G. Poletto, A. C. Sterling, M. Romoli, *Astrophys. J.* **793**, 86 (2014).
21. N.-E. Raouafi, G. Stenborg, *Astrophys. J.* **787**, 118 (2014).
22. V. M. Uritsky *et al.*, *Astrophys. J.* **907**, 1 (2021).
23. P. Kumar *et al.*, *Astrophys. J.* **933**, 21 (2022).
24. N. E. Raouafi *et al.*, *Astrophys. J.* **945**, 28 (2023).
25. I. A. Ahmad, G. L. Withbroe, *Sol. Phys.* **53**, 397–408 (1977).
26. Y.-M. Wang, *Astrophys. J.* **435**, L153 (1994).
27. S. Patsourakos, J.-C. Vial, *Astron. Astrophys.* **359**, L1–L4 (2000).
28. L. Teriaca, G. Poletto, M. Romoli, D. A. Biesecker, *Astrophys. J.* **588**, 566–577 (2003).
29. N. Fargette *et al.*, *Astrophys. J.* **919**, 96 (2021).
30. P. Rochus *et al.*, *Astron. Astrophys.* **642**, A8 (2020).
31. D. Müller *et al.*, *Astron. Astrophys.* **642**, A1 (2020).
32. Materials and methods are available as supplementary materials.
33. F. Moreno-Insertis, K. Galsgaard, I. Ugarte-Urra, *Astrophys. J.* **673**, L211–L214 (2008).
34. K. Shibata *et al.*, *Science* **318**, 1591–1594 (2007).
35. A. C. Sterling, R. L. Moore, D. A. Falconer, M. Adams, *Nature* **523**, 437–440 (2015).
36. S. Mandal *et al.*, *Astron. Astrophys.* **664**, A28 (2022).
37. L. P. Chitta, A. R. C. Sukarmadji, L. Roupe van der Voort, H. Peter, *Astron. Astrophys.* **623**, A176 (2019).
38. L. D. Xia, E. Marsch, W. Curdt, *Astron. Astrophys.* **399**, L5–L9 (2003).
39. G. L. Withbroe, *Astrophys. J.* **325**, 442 (1988).
40. E. N. Parker, *Astrophys. J.* **330**, 474 (1988).
41. K. L. Harvey, F. Recely, *Sol. Phys.* **211**, 31–52 (2002).
42. T. Sakao *et al.*, *Science* **318**, 1585–1588 (2007).
43. G. A. Doschek *et al.*, *Astrophys. J.* **667**, L109–L112 (2007).
44. L. K. Harra *et al.*, *Astrophys. J.* **676**, L147–L150 (2008).
45. D. H. Brooks *et al.*, *Astrophys. J.* **917**, 25 (2021).
46. Y.-M. Wang, in *Cool Stars, Stellar Systems, and the Sun*, R. A. Donahue, J. A. Bookbinder, Eds., vol. 154 of *Astronomical Society of the Pacific Conference Series* (1998), pp. 131–152.
47. S. Parhi, S. T. Suess, M. Sulkanen, *J. Geophys. Res.* **104**, 14781–14787 (1999).
48. J. Andries, M. Goossens, *Astron. Astrophys.* **368**, 1083–1094 (2001).
49. Th. Roudier, R. Muller, *Sol. Phys.* **107**, 11–26 (1986).
50. G. W. Simon, N. O. Weiss, *Z. Astrophys.* **69**, 435–450 (1968).
51. B. Mampaey *et al.*, SolO/EUI Data Release 5.0 2022-04 (Royal Observatory of Belgium, 2022); <https://doi.org/10.24414/2qfw-tr95>.
52. I. Zouganelis *et al.*, *Astron. Astrophys.* **642**, A3 (2020).

ACKNOWLEDGMENTS

Solar Orbiter is a space mission with international collaboration between ESA and NASA, operated by ESA. The EUI instrument was built by CSL, IAS, MPS, MSSL/UCL, PMOD/WRC, ROB, and LCF/IO with funding from the Belgian Federal Science Policy Office (BELSPO/PRODEX PEA 4000134088), the Centre National d'Etudes Spatiales (CNES), the UK Space Agency (UKSA), the Bundesministerium für Wirtschaft und Energie (BMWi) through the Deutsches Zentrum für Luft- und Raumfahrt (DLR), and the Swiss Space Office (SSO). This research has made use of NASA's Astrophysics Data System. **Funding:** L.P.C. acknowledges funding by the European Union (ERC, ORIGIN, 101039844). S.P. acknowledges funding by CNES through the Multi Experiment Data & Operation Center (MEDOC). D.M.L. thanks the Science and Technology Facilities Council for the award of an Ernest Rutherford Fellowship (ST/R003246/1). A.N.Z., D.B., E.K., L.R., and C.V. thank the Belgian Federal Science Policy Office (BELSPO) for the provision of financial support in the framework of the PRODEX Programme of the European Space Agency (ESA) under contract nos. 4000134474 and 4000136424. **Author contributions:** L.P.C. led the study and data analysis and wrote the manuscript with inputs from A.N.Z., D.B., H.P., S.P., S.M., R.A.C., U.S., L.T., É.B., D.M.L., and D.B.S. F.A., E.K., and C.V. contributed to data reduction. A.N.Z. led the Solar Orbiter observing campaign. D.B. is the principal investigator of EUI. All authors discussed and interpreted the results. **Competing interests:** The authors declare no competing interests. **Data and materials availability:** The HRI_{EUV} level-2 data are archived by the Royal Observatory of Belgium (5I). We used observations in the time range of 30 March 2022 04:30 to 05:00 UT (files from solo_L2_eui-hrievnon-image_20220330T043000227_V01.fits to solo_L2_eui-hrievnon-image_20220330T045957224_V01.fits). The data can alternatively be retrieved from ESA's Solar Orbiter Archive <https://soaresac.esa.int/soar/> using the same time range and the Solar Orbiter Observing Plan (SOOP) (52) name "R_SMALL_HRES_MCAD_Polar-Observations." **License information:** Copyright © 2023 the authors, some rights reserved; exclusive licensee American Association for the Advancement of Science. No claim to original US government works. <https://www.science.org/about/science-licenses-journal-article-reuse>. This research was funded in whole or in part by the European Union through Horizon Europe (grant no. 101039844), a cOAlition S organization. The author will make the Author Accepted Manuscript (AAM) version available under a CC BY public copyright license.

SUPPLEMENTARY MATERIALS

science.org/doi/10.1126/science.ade5801
Materials and Methods
Supplementary Text
Figs. S1 to S9
Tables S1 to S4
References (53–75)
Movies S1 to S12

Submitted 25 August 2022; accepted 14 July 2023
10.1126/science.ade5801



Picoflare jets power the solar wind emerging from a coronal hole on the Sun

L. P. Chitta, A. N. Zhukov, D. Berghmans, H. Peter, S. Parenti, S. Mandal, R. Aznar Cuadrado, U. Schhle, L. Teriaca, F. Auchre, K. Barczynski, . Buchlin, L. Harra, E. Kraaikamp, D. M. Long, L. Rodriguez, C. Schwanitz, P. J. Smith, C. Verbeeck, and D. B. Seaton

Science, **381** (6660), .

DOI: 10.1126/science.ade5801

Editor's summary

Plasma is constantly streaming away from the Sun, forming the solar wind. A likely source of this plasma is coronal holes, regions of the Sun's corona with magnetic field lines that open outward. Chitta *et al.* observed a coronal hole in the extreme ultraviolet using the Solar Orbiter spacecraft and identified several types of small-scale jets within it (see the Perspective by Ugarte-Urra and Wang). Large numbers of jets occurred during the observation, but each one lasted only a few dozen seconds. The authors calculated that the jets provide enough energy and plasma to supply a large fraction of the solar wind, at least during quiet periods. —Keith T. Smith

View the article online

<https://www.science.org/doi/10.1126/science.ade5801>

Permissions

<https://www.science.org/help/reprints-and-permissions>

Use of this article is subject to the [Terms of service](#)

Science (ISSN) is published by the American Association for the Advancement of Science. 1200 New York Avenue NW, Washington, DC 20005. The title *Science* is a registered trademark of AAAS.

Copyright © 2023 The Authors, some rights reserved; exclusive licensee American Association for the Advancement of Science. No claim to original U.S. Government Works